1   # ThruTracker: Open-Source Software for 2-D and 3-D Animal Video

2   # Tracking

3   Aaron J. Corcoran[1*], Michael R. Schirmacher[2], Eric Black[3] and Tyson L. Hedrick[4]

4   [1]Department of Biology, 1420 Austin Bluffs Blvd, University of Colorado, Colorado Springs, Colorado,
5   USA

6   [2]Bat Conservation International, 500 N Capital of TX Hwy. Bldg. 1. Austin, Texas, USA

7   [3]Canebrake Environmental Services, LLC. 7405 New Forest Lane, Wake Forest, NC 27587

8   [4]Department of Biology, University of North Carolina, 120 South Road, Chapel Hill, North Carolina, USA

9

10   Correspondence: Aaron Corcoran, email: acorcora@uccs.edu

11

12   Running headline: Open-source Animal Tracking Software

13   **Abstract**

14   1. Tracking animal movement patterns using videography is an important tool in many biological

15   disciplines ranging from biomechanics to conservation. Reduced costs of technology such as

16   thermal videography and unmanned aerial vehicles has made video-based animal tracking more

17   accessible, however existing software for processing acquired video limits the application of

18   these methods.

19   2. Here, we present a novel software program for high-throughput 2-D and 3-D animal tracking.

20   ThruTracker provides tools to allow video tracking under a variety of conditions with minimal

21   technical expertise or coding background and without the need for paid licenses. Notable

22   capabilities include calibrating the intrinsic properties of thermal cameras; tracking and counting

23   hundreds of animals at a time; and the ability to make 3-D calibrations without dedicated

24   calibration objects. Automated 2-D and 3-D workflows are integrated to allow for analysis of

25   largescale datasets.

26   3. We tested ThruTracker with two case studies. The 2-D workflow is demonstrated by counting

27   bats emerging from bridges and caves using thermal Videography. Tests show that ThruTracker

28   has a similar accuracy compared to humans under a variety of conditions. The 3-D workflow is

29   shown for making accurate calibrations for tracking bats and birds at wind turbines using only

30   the wind turbine itself as a calibration object.

31   4. ThruTracker is a robust software program for tracking moving animals in 2-D and 3-D. Major

32   applications include counting animals such as bats, birds, and fish that form large aggregations,

33   and documenting movement trajectories over medium spatial scales (~100,000 m^3). When

34   combined with emerging technologies, we expect videographic techniques to continue to see

35   widespread adoption for an increasing range of biological applications.

36   **Key words**: Animal Flight, Animal Movement, Movement Ecology, Population Monitoring, Flight

37   Biomechanics, Video Detection

38   1. Introduction

39   Video-based animal tracking is a widely used tool in fields as diverse as biomechanics, animal behavior,

40   ecology, and population monitoring (Dell et al., 2014). The reduced price of thermal video cameras,

41   high-speed cameras, and other technologies such as unmanned aerial vehicles (UAVs) has expanded

42   dramatically the capabilities of investigators studying animal movement in the lab and in the field

43   (Jackson, Evangelista, Ray, & Hedrick, 2016). This has placed great demand for video processing

44   software.

45   Various video tracking tools are available for two-dimensional (2-D), and three-dimensional (3-D) animal

46   tracking. Two-dimensional tracking is often used for studies of one or multiple individuals under

47   controlled laboratory settings. Two-dimensional tracking can also be useful for surveying animal

48   populations such as bats or birds and for monitoring their migratory behavior (Kunz et al., 2009).

49   Algorithms differ in how they detect animals and how they connect detections between frames to form

50   spatiotemporal tracks. For example, some software uses background subtraction for detection

51   (Rodriguez et al., 2018) while other programs use adaptive thresholding (Sridhar et al., 2019). One

52   popular program uses image recognition to help track individuals (Pérez-Escudero et al. 2014). Deep

53   learning based approaches have recently become popular, particularly for marker-less tracking of animal

54   body parts (Mathis et al., 2018; Pereira et al., 2019).

55   Three-dimensional animal tracking uses two or more cameras to triangulate animal positions. This

56   requires synchronized video acquisition, careful calibration of the optical properties of cameras

57   [i.e.2camera extrinsics). Several software programs are available for generating 3-D calibrations and

58   tracking animals in 3-D (Noldus et al., 2001; Hedrick, 2008; Theriault et al., 2014; Jackson et al., 2016;

59   Knorlein et al., 2016; Nath et al., 2019).

60   Originally, 3-D calibrations required that an object with several markers at known 3-D positions be

61   placed within the field of view of each camera (Abdel-Aziz & Karara, 1971). More recent workflows

62   produce calibrations by moving an object with a recognizable 2-D pattern ["checkerboard calibration"

63   (Zhang, 2000)] or with two markers at a fixed distance ("wand calibration") through the calibration

64   volume (Theriault et al., 2014). This allows one to set the scale of the scene using the wand length or

65   pattern scale and to estimate the accuracy of the calibration based on the variation of reconstructed

66   wand lengths. However, researchers are increasingly interested in studying animals within large volumes

67   in the natural environment where it is difficult to deploy calibration objects or where doing so might

68   disturb the animals under study (Evangelista, Ray, Raja, & Hedrick, 2017; Corcoran & Hedrick, 2019). In

69   addition, much of the currently available 3-D tracking software requires manual digitization of objects in

70   the videos, which limits the amount of data that can be processed. Finally, calibration procedures are

71   not widely available for determining the intrinsic properties of thermal cameras, preventing their

72   widespread use for 3-D tracking applications.

73   Here we present ThruTracker, a free and open-source software package for high-throughput 2-D and 3-

74   D animal tracking. ThruTracker provides an app-based environment (i.e., no coding required) with all the

75   tools necessary to track animals under a variety of conditions with light-based or thermal cameras.

76   ThruTracker is coded in MATLAB v2020b (Natick, MA, USA) and compiled versions of the software are

77   provided so that it can be installed and run for free without any licenses. We provide source code under

78   a 3-clause BSD license for those who may want to customize the software for their own purposes.

79   ThruTracker is also compatible with any tracking software that outputs 2-D coordinates, and it exports

80   data in standard text formats that can be imported into other software for further processing or

81   statistical analysis.

82   We first provide an overview of the 2-D and 3-D track generation process, before demonstrating the use

83   of ThruTracker with two test cases—tracking bats at wind turbines and counting bat emergences from

84   bridges and caves using a thermal camera flown with an Unmanned Aerial Vehicle (UAV) or recording

85   from the ground. We conclude by discussing applications of 3-D tracking and current limitations. A step-

86   by-step manual for ThruTracker along with additional recommendations for camera setups and use of

87   the software is available on our website (www.sonarjamming.com/thrutracker).

88   2. Materials and Methods

89   2.1 Workflow for 2-D and 3-D Tracking

90   ThruTracker can be used either for 2-D or 3-D video tracking. Two-dimensional tracking does not require

91   that the videos be calibrated and is therefore a much simpler procedure. Three-dimensional tracking

92   requires calibration of the camera properties such as focal length and lens distortion (intrinsic

93   calibration) and determination of the positions and orientations of the cameras for each scene where

94   they are deployed (extrinsic calibration). The workflow for 3-D track generation is shown in Figure 1.
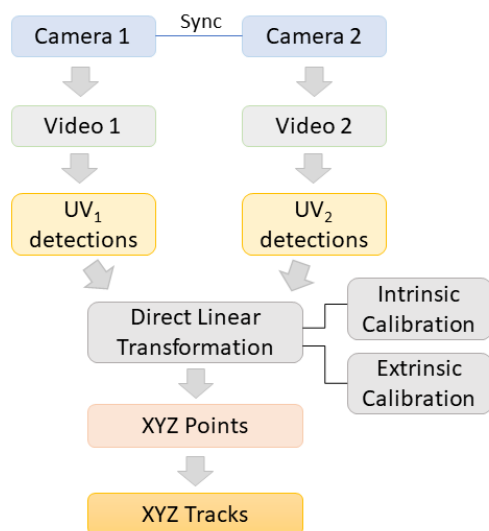

Figure 1. Overview of 3-D track generation procedure. Two or more cameras acquire synchronized video, which are each processed to generate 2-D (UV) detections. Intrinsic and extrinsic camera calibrations are used to generate direct linear transformation (DLT) equations that transform UV coordinates into real-world 3-D or XYZ points for each detection. XYZ points are then stitched together across frames to generate 3-D tracks.

95

96   Step 1: Video Acquisition. Synchronized videos are acquired using two or more cameras. Some cameras,

97   such as FLIR A65 thermal video cameras (FLIR Systems, Inc., Wilsonville, OR) used in our testing, have

98   dedicated electronic inputs that allow digital signals to synchronize the shutters of each camera. An

99   alternative for cameras without sync ports is to use audio signals that are broadcast to each camera

100   (Jackson et al., 2016). Audio synchronization of cameras does not allow for shutter synchronization,

101   therefore there will be a time offset of up to half the frame rate even after synchronization. Recording

102   at 30 Hz, a half-frame synchronization accuracy has been sufficient to achieve highly accurate

103   calibrations for animals moving at low to moderate pixel speeds (Corcoran & Hedrick, 2019). Audio

104   synchronization may also require fine-tuning since some camera models may not keep the audio and

105   video outputs in perfect alignment.

106   Step 2: Object detection. After videos are acquired, videos from each camera are processed to detect

107   moving objects in each frame. ThruTracker uses a Gaussian mixture-based background subtraction

108   algorithm implemented in OpenCV ["BackgroundSubtractorMOG2", (Zivkovic, 2004; Zivkovic & Van Der

109   Heijden, 2006)]. A blob detector is then used to isolate detections and the blob centroids are used as

110   detection coordinates. A simplified interface allows the user to rapidly select and modify detection

111   settings for their application. Settings include: 1) selecting which frames to process, 2) minimum and

112   maximum object size in pixels, 3) sensitivity for adjusting the threshold for discriminating foreground

113   from background, 4) Number of background frames used for generating the rolling background image,

114   and 5) target object diameter. This last option determines the size of a 2-D gaussian filter that is applied

115   to the image, which helps reduce noise and isolate closely spaced animals. Each frame of the video is

116   processed for detections before detections are linked together into 2-D or 3-D tracks in the proceeding

117   steps. Two-dimensional tracking applications can skip to step 6.

118   Step 3: Intrinsic camera calibration. For 3-D tracking applications, one must determine the camera's

119   intrinsic properties, including the focal length, principal point and lens distortion (Abdel-Aziz & Karara,

120   1971; Hartley & Zisserman, 2004; Lourakis & Argyros, 2009). This information can be used to map any

121   pixel in the camera image into a vector in a camera-based frame. Typically, this calibration can be done

122   once per camera and lens combination in a laboratory and the values should be similar between

123   cameras and lens of the same make and model. In some special circumstances one might need to

124   calibrate each individual camera-lens pair for increased accuracy. Cameras with variable focal length

125   (i.e., a zoom lens) typically need to be calibrated separately at each focal length used for recording.

126   We use MATLAB's built-in camera calibratio functions (Bouguet, 1999) with some modifications to

127   calibrate thermal images (Yahyanejad, Misiorny, & Rinner, 2011). We recommend using MATLAB's built-

128   in camera calibrator app or freely available functions in OpenCV or Argus (Jackson et al., 2016) for

129   calibrating light-based cameras.

130   Traditionally, calibration procedures for light-based cameras rely on detecting the corners of a

131   checkerboard pattern. With thermal imaging, one must first heat the checkerboard so that the darker

132   squares will be hotter than the lighter squares because of higher light absorption (Figure 2a). For

133   example, we achieved this by moving two 100-watt lamps over the checkerboard pattern for about 20
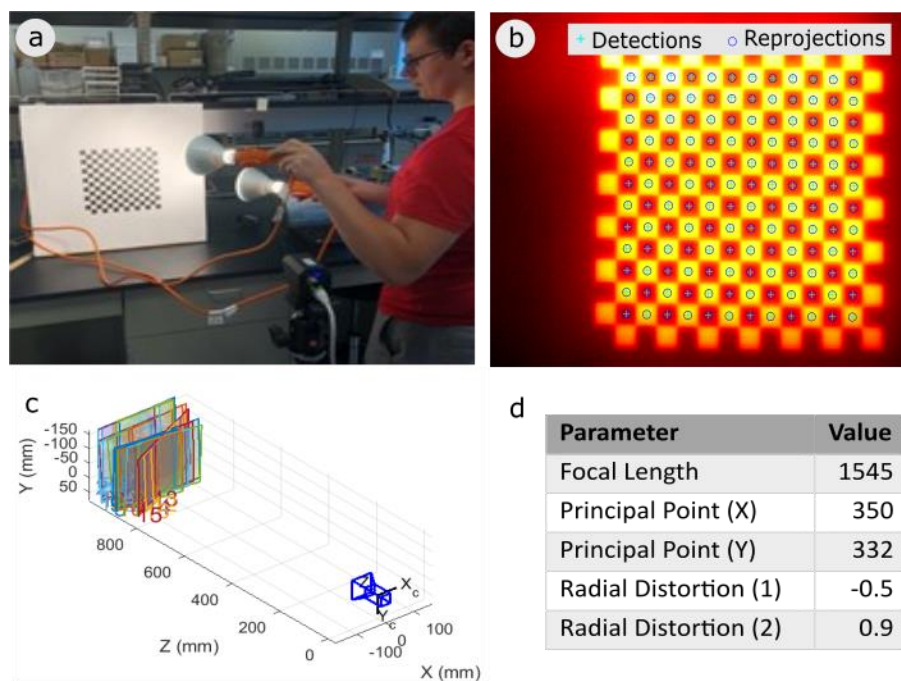
134   seconds before taking thermal images.

Figure 2. Thermal camera intrinsic calibration. (a) An experimenter heats a checkerboard pattern with two 100-watt lamps. (b) Example thermal image of a checkerboard pattern with detected and reprojected square centers. (c) Graphical depiction of the camera and 28 images of the checkerboard pattern taken at different positions and orientations. (d) Example output of intrinsic camera parameters for a Flir A65 camera.

Parameter	Value
Focal Length	1545
Principal Point (X)	350
Principal Point (Y)	332
Radial Distortion (1)	-0.5
Radial Distortion (2)	0.9

135

136   However, uneven heating combined with rapid conduction of heat through the checkerboard image

137   increases the difficulty of detecting the corners between light and dark squares (or in this case between

138   cold and hot squares; Figure 2b). Instead of detecting the corners, the cooler portions of the image are

139   dilated so that each hot square is reduced in size and no longer connected to adjacent hot squares. A

140   blob-detector is then used to detect the centers of the hot squares. The pixel values of the image are

141   then inverted, and the procedure is repeated to detect the centers of the cold squares. This is repeated

142   for 20-30 images taken at different positions and orientations relative to the camera. The resulting data

143   are used by the software to calculate the camera's intrinsic parameters (Figure 2c, d).

144   Step 4: Extrinsic camera calibration. A second calibration procedure is required for generating 3-D tracks

145   for each recording setup—that is, any time the cameras are moved even slightly. The extrinsic

146   calibration determines the positions of the cameras in real-world 3-D space and their orientations [roll,

147   yaw and pitch; (Abdel-Aziz & Karara, 1971)]. Together with the intrinsic calibration data, the extrinsic

148   calibration allows one to map objects that are detected in two or more cameras to real-world 3-D

149   coordinates.

150   As noted previously, there are several approaches for generating extrinsic calibrations. ThruTracker has

151   two options: a wand-based procedure that is based on methods used for easyWand (Lourakis & Argyros,

152   2009; Theriault et al., 2014) and a procedure that is based exclusively on background points. One can

153   also import calibrations made using DLTdv or easyWand (Hedrick, 2008; Theriault et al., 2014).

154   Background points include any object that is visible within both cameras such as tips of tree branches,

155   wind turbines, or animals. Moving objects can be used if the images are taken synchronously between

156   cameras. This background point procedure [also known as structure from motion (Schönberger &

157   Frahm, 2016)] means that 3-D calibrations can be made without dedicated calibration objects within the

158   field of view. In effect, any object visible by two or more cameras can be used as a calibration object.

159   Two additional components of the calibration must be determined when no dedicated calibration

160   objects are used: the scale of the scene and the gravitational axis. The scale can be set by specifying two

161   points in the scene that are at a known distance from one another. Alternatively, one can use the

162   distance between cameras to set the camera scale.

163   Second, the gravitational axis can be set by measuring the inclination angle of one of the cameras using

164   an inclinometer. This value is input into ThruTracker's calibration app during the calibration procedure.

165   With these options, one can obtain calibration data rapidly in the field with only a few measurements

166   and with no requirement for deploying calibration objects. This is especially helpful for situations where

167   it is not feasible to deploy calibration objects or where their use would disturb animals under study.

168   A notable down-side of not using calibration objects is the absence of objects at known positions that

169   can be used to check the accuracy of the calibration. Therefore, it is important to conduct tests of the

170   calibration procedure using objects at known distances. For example, in our test using wind turbines

171   below, we measured the variation in the reconstructed lengths of the turbine blades at different times

172   and positions throughout our recording. Another alternative would be to conduct test setups in the field

173   at locations where it is easier to deploy calibration objects such as a wand.

174   Step 5: Generating 3-D Points. Three-dimensional points are generated after objects have been detected

175   in videos from each camera and intrinsic and extrinsic calibrations are completed. For each set of

176   synchronized video frames, theoretical 3-D points are created from all combinations of 2-D detections

177   across cameras. Each putative 3-D point has an associated direct linear transformation (DLT) residual.

178   The DLT residual is the distance in pixels between the observed image coordinates of a marker and the

179   "ideal" image coordinates computed from the estimated 3-D location of the marker and the calibration

180   information for the camera that captured the image. If we visualize each 2-D detection as a vector in 3-D

181   space with its origin at the camera, the residuals indicate how closely a given set of 2-D detections and

182   their associated vectors come to crossing in 3-D space. The algorithm starts by creating 3-D points based

183   on sets of 2-D points with the lowest residuals and removing those points from the available pool. It

184   proceeds until there are no more 3-D points with residuals below the specified threshold.

185   Step 6: Generating 2-D and 3-D Tracks. Two-dimensional and Three-dimensional points are stitched

186   together across frames to make tracks. Each 2-D or 3-D point in the first frame is a putative track.

187   Detections in each proceeding frame are assigned to existing tracks, or if no assignment is made, they

188   become the beginning of a new track. A Kalman filter is applied to each track to predict the position of

189   the track in the next frame. The distance between each detection and the predicted positions are

190   computed. This is done both in 2-D and in 3-D to calculate a cost matrix. A Hungarian algorithm is used

191   to determine the combination of assignments that minimizes cost across the assignment matrix (Kuhn,

192   1955). Finally, a threshold is specified in ThruTracker such that assignments are only made if their cost is

193   below the threshold. One can specify the number of frames between detections that are allowed (i.e.,

194   gap distance) before a track is terminated. One also specifies the minimum number of detections

195   required for a track to be retained. Longer gaps and smaller minimum numbers of detections increase

196   the number of tracks that are retained but increases the number of false positive tracks generated from

197   noise.

198   Step 7: Data visualization, analysis and classification: ThruTracker offers multiple tools for visualizing and

199   processing tracks. One can rapidly toggle between tracks and use shortcut keys to classify them into

200   different categories. For example, for wind turbine applications, the tracks can be labeled "bird", "bat",

201   "airplane", "noise", etc. Another option allows all the tracks to be visualized at once. Tracks can then be

202   selected as groups and classified based on their positions, start or end points. This tool is helpful for

203   selecting tracks based on their location, as exhibited in the bat emergence case study presented below.

204   Another option allows the user to draw a rectangle over the camera image to count exits and re-entries

205   as animals pass into or out of the rectangle. This is useful, for example, when counting bats exiting a

206   cave roost. Resulting 2-D, 3-D and track data can be exported into CSV files for use in other analysis

207   programs.

2.2 Case Studies

2.2.1 Case Study 1: Counting bat exits from bridges and caves using thermal imaging.

210   We used ThruTracker to count bats emerging from bridges using a DJI Zenmuse XT2 thermal camera

211   with a 13 mm lens (45-degree field of view) suspended from a DJI Matrice 300 drone (SZ DJI Technology

212   Co., Shenzhen, China). Because this analysis was done in 2-D there was no need for intrinsic or extrinsic

213   calibrations. The drone was flown at altitudes of 50 m and 80 m above a bridge known to be a roost

214   location for big brown bats (*Eptesicus fuscus*) in August of 2020 near Burnsville, NC, USA. We also

215   counted gray bats leaving caves using thermal cameras placed at ground level. Videos of gray bats were

216   provided by the US Fish and Wildlife Service.

217   Our goals were 1) to determine the maximum distance at which bats could be detected and 2) to

218   compare manual counts of emergences with those produced using ThruTracker. The bridge recordings

219   provide a test of relatively low numbers of bats counted near the limits of their detection range. The

220   cave recordings test detection of large numbers with high rates of occlusion.

221   Videos were processed in ThruTracker with the following parameters: sensitivity, 35; background

222   frames, 20; Min object pixels, 1; max object pixels 100; min track length 5, max gap length 5; match

223   threshold 10. After detections were made in ThruTracker, the applet TrackSelector was used to rapidly

224   select tracks that originated near the edge of the bridge. Manual observers used VirtualDub software to

225   play videos at 50% of normal speed and paused and reviewed videos frame by frame, as necessary.

226   We processed two videos taken at heights of 50 m and 80 m above the bridge and two videos

227   representing different bat densities at caves (Table 1). Videos were not meant to census the entire

228   emergences, but rather provide data for comparing detection abilities.

2.2.2 Case Study 2:

229

230 We tested ThruTracker's ability to make 3-D calibrations for tracking 3-D flights of bats and birds at wind

231 turbines. Studying animal movements at wind turbines is a problem of considerable interest, especially

232 for bats who are being killed in large numbers for mostly unknown reasons (Arnett & Baerwald, 2013).

233 Thermal imaging has been used for studying bats at wind turbines in 2-D (Horn, Arnett, & Kunz, 2008;

234 Cryan et al., 2014) and 3-D (Kinzie et al., 2018; Schirmacher, 2020). Proprietary software for 3-D tracking

235 of bats at wind turbines (was also recently published (Matzner, Warfel, & Hull, 2020). Here we report on

236 our field camera setup, intrinsic and extrinsic calibration. Because we conducted these tests under cold

237 winter conditions with few bats or birds present, we did not obtain 3-D animal tracks. For example

238 tracks using a similar approach, see Schirmacher, 2020 (Schirmacher, 2020).

239 We tested the calibration setup using two Flir A65 thermal cameras with 25-degree lenses synchronized

240 with electronic inputs at an experimental wind turbine at the National Renewable Energy Laboratory

241 (NREL) in Golden, CO during December 2019. The cameras were placed 33 m apart from one another

242 and 40 m from the base of the turbine's monopole. Cameras were aimed slightly below the wind

243 turbine's nacelle, which was 80 m off the ground. This resulted in an inclination angle of 62.2 degrees for

244 our reference camera.

3. Results

245

3.1 Case Study 1: Counting bat exits from bridges and caves using thermal imaging.

246

247 ThruTracker detected similar numbers of bats compared to the manual observers in all test cases, with

248 error rates of 0.6-7.1% (Table 1; Figure 1; Supplemental Video 1. Thermal video taken from a UAV

249 showed that the 50 m recording height was comfortably within the detection range for the bats. Bat

250 detections had a size of 5.2 ± 3.4 pixels (mean ± st. dev.) and tracks extended across most of the image

251 (Figure 3a) including over water and over the bridge. However, bats failed to be tracked over some land

252   areas where they lacked contrast with the background (e.g., see tracks terminating as they approach

253   land area in bottom right portion of Figure 3a). Manual inspection of videos at these locations found

254   that bats were not readily visible to the human eye, so this appears to be a limitation of the thermal

255   imaging, not the detection algorithm.

256   The 80 m recording height was much closer to the detection limit for *E. fuscus* bats using this recording

257   setup. Bats had a detection size of 1.9 ± 1.1 pixels. Visual inspection of videos revealed that bats were

258   only barely visible and that they were not detectable to the human eye within a short distance of their

259   emergence. This is reflected in the ThruTracker tracks that terminate over open water some distance

260   from the bridge exits (Figure 3b). This may have resulted from bats dropping to a lower altitude (and

261   further distance from the camera) as they left the bridge, as was visible in other camera views taken at

262   an oblique angle relative to the ground. ThruTracker performed slightly worse under these at the 80 m

263   height than the 50 m height, but still detected 93% of tracks that were detected manually (Table 1).

264   Counts of gray bats (*Myotis grisescens*) exiting caves were used to test of ThruTracker's multi-object

265   tracking abilities. ThruTracker achieved error rates of 4.3% and 0.6% for the two test videos, which we

266   estimated to have exit rates of 16.4 and 103.0 bats per second (Table 1; Figure 3c, d; Supplemenatal

267   Video 2).

268   *Table 1. Comparison of manual and automated bat counts using thermal videography*

	Video 1	**Video 2**	**Video 3**	**Video 4**
Emergence type	Bridge	Bridge	Cave	Cave
Camera height (m)	50	80	ground	ground
Duration (m:ss)	3:21	1:58	0:05	0:05
ThruTracker detections	86	39	85	518
Manual detections*	85.5 (85,86)	42 (42,42)	81.5 (81, 82)	515 (508,522)
Exit rate (bats per second)	0.42	0.35	16.4	103.0
Error rate	0.6%	7.1%	4.3%	0.6%

269   *Values show means of 2 observers; values in parentheses show values of the two observers.

Figure 3 Example ThruTracker detections of bats leaving a bridge (a, b) and cave (c, d). Big brown bats (*Eptesicus fuscus*) were filmed exiting a bridge using a thermal camera on a UAV flying at 50 m (a) and 80 m altitude (b). Red tracks indicate exits and white tracks indicate other detections. In (a, b) circles indicate the starting point of tracks to highlight departures from the bridge and the entirety of all tracks are shown. In (c, d) detections from a single frame are shown (circles) with tracks indicating movement over the two previous frames. See table 1 for statistics.

270

271
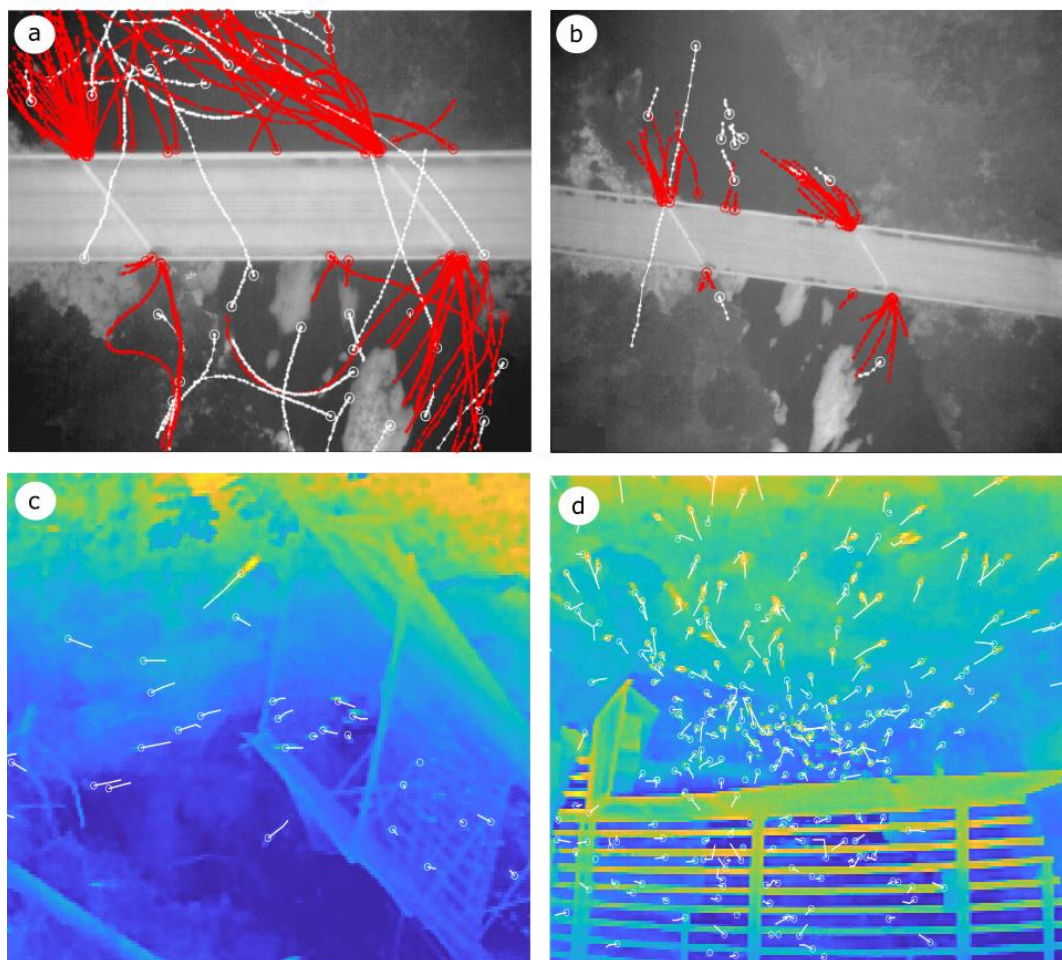
3.2 Case Study 2: Calibrating large 3-D volumes using wind turbines.

In our second case study, we demonstrate ThruTracker's 3-D workflow for calibrating large spatial

volumes using only the turbine itself as a calibration object. We calibrated the FLIR A65 thermal cameras

275   (640 x 512 pixel resolution) using the intrinsic calibration method described above. Example images and

276   resulting intrinsic camera parameters are shown in Figure 2. We used 28 checkerboard images, with an

277   average reprojection residual error of 0.69 pixels (range 0.48-0.83 pixels).

278   We generated an extrinsic calibration in ThruTracker using 67 points from the wind turbine as

279   background points (Figure 3). These included hot spots, corners and an anemometer on the nacelle, and

280   turbine blade tips. Points were digitized manually using DLTdv8 (Hedrick, 2008). Efforts were made to

281   select points that were 1) clearly visibly in both cameras, 2) distinct points in 3-D space, such as small

282   hot spots or sharp edges of objects, and 3) covering a broad range of 2-D and 3-D positions. We

283   excluded six points because they had DLT residuals > 3 pixels. The remaining calibration had mean

284   reprojection errors of 0.63 pixels.

285   We set the scale of the scene using the distance between the two cameras (33 m) and the gravitational

286   axis was set using the inclination angle of the second camera (62.2 degrees). The resulting calibration

287   had a volume of 235,597 m^3 assuming a maximum detection distance of 200 m. The maximum detection

288   range is likely less than 200 m for small bats (<30 g) with this camera setup, but it is possible that some

289   large birds could be detected at this distance.

290   To test the spatial accuracy of our calibration, we measured the distance between the tips of turbine

291   blades and the tip of the hub in 23 frames chosen to represent a variety of spatial configurations. This

292   resulted in a mean distance of 41.4 m, standard deviation of 1.05 m, and coefficient of variation of 0.02.

293   Therefore, we can expect typical errors less than ± 1-2 m for this calibration setup. For comparison, a

294   recently published study testing similar software for tracking birds and bats at wind turbines found

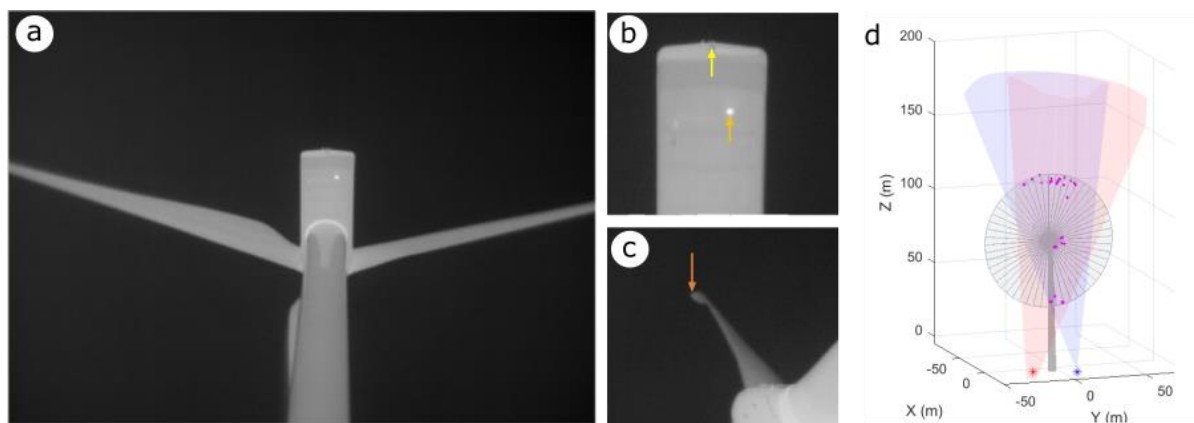295   errors up to ± 20 m (Matzner et al., 2020).

Figure 4. Extrinsic calibration of a wind turbine scene. (a) Example views from a single camera. (b, c) Examples of background points used for generating the calibration. These include a back corner of the nacelle (yellow arrow), a small hotspot of unknown origin (orange arrow) and a turbine tip (dark orange arrow). (d) Visualization of the calibrated scene. Views of two cameras are shown in light red and light blue shading. The wind turbine is shown as a grey outline but note that the turbine rotates about the vertical axis depending on wind direction. Magenta points show 3-D positions of points used for making the calibration.

4. Discussion

4.1. Animal Tracking Applications

Videographic techniques are seeing expanded use for studies of wildlife (Cilulko, Janiszewski, Bogdaszewski, & Szczygielska, 2013; Christiansen et al., 2014; Gonzalez et al., 2016) ranging from animals in agricultural fields (Christiansen et al., 2014), to cetaceans (Seymour, Dale, Hammill, Halpin, & Johnston, 2017), bats and birds (Betke et al., 2008; Cullinan, Matzner, & Duberstein, 2015; Matzner, Cullinan, & Duberstein, 2015) and ants (Narendra & Ramirez-Esquivel, 2017). One major application of videography for studies of animals in the natural environment is counting populations. For example, 3-D thermal imaging has been used to show that bat colonies have only a small fraction of the number of individuals compared to earlier human counts (Betke et al., 2008). Thermal imaging has also been used in combination with radar and acoustics for monitoring migratory patterns of birds (Gauthreaux & Livingston, 2006; Horton, Shriver, & Buler, 2015).

310   A second major application of videography is studying animal movement patterns. Numerous studies

311   have investigated the structure and rules underlying bird flocks (Ballerini et al., 2008; Evangelista et al.,

312   2017) and schools of fish (Jolles et al., 2017). Videography has also been used for studying flight

313   biomechanics of animals under natural conditions et al., 2015), and interactions between bats and birds

314   and large structures such as wind turbines and oil and gas platforms (Horn et al., 2008; Cryan et al.,

315   2014; Ronconi et al., 2015). Most of the studies described above have relied on custom software that is

316   not widely available. The aim of the current study was to develop a robust, easy to use and free

317   software package that could be used for these and other applications.

318   4.2 ThruTracker Capabilities

319   Here we present a new software package for 2-D and 3-D animal tracking. ThruTracker has several

320   features not found in other freeware. These include easily adjustable procedures for 2-D and 3-D

321   tracking; a tool for calibrating intrinsic parameters of thermal cameras; the ability to track and count

322   hundreds of animals simultaneously; and the ability to make 3-D calibrations without dedicated

323   calibration objects. We demonstrate these capabilities by counting bats leaving bridges and caves (Table

324   1; Figure 3) and making a 3-D calibration using only a wind turbine as a calibration object (Figure 4).

325   The software is compatible with thermal and light-based imaging and most standard video formats (e.g.,

326   avi, wmv, mp4). ThruTracker uses an app-based environment with no coding required to make well-

327   established detection and tracking algorithms widely available. Users simply import videos and select

328   the detection and tracking options. These features make it easy to track moving animals under a variety

329   of conditions.

330   4.3 Requirements and Limitations

331   ThruTracker uses a well-established background subtraction algorithm for object detection (Zivkovic,

332   2004; Zivkovic & Van Der Heijden, 2006). This method generates a rolling model of the background using

333   a number of frames that can be specified by the user. This approach is best suited for stationary

334   backgrounds and animals that are in near continuous motion. It has difficulty with animals that stay in

335   one place; however, using more images for generating the background would help address this problem.

336   ThruTracker aims to detect one point for each animal (the blob centroid). For detecting multiple body

337   parts per animal one should consider deep-learning based approaches (Mathis et al., 2018; Pereira et al.,

338   2019). ThruTracker has built-in compatibility for importing detections from other programs such as

339   DeepLabCut (Mathis et al., 2018) for could be used for generating 3-D tracks from point clouds.

340   The main requirements for tracking in 3-D are 1) synchronized video are acquired from at least two fixed

341   cameras 2) camera intrinsics are calibrated in the laboratory, and 3) some objects (including the focal

342   animals themselves) are visible at a range of 2-D and 3-D positions within the calibrated volume.

343   Without the requirements for dedicated calibration objects, it is now possible to calibrate nearly any

344   volume in the lab or field. We demonstrate this workflow for generating 3-D calibrations at wind

345   turbines, where it would be logistically challenging to put calibration objects in the airspace (Figure 4).

346   Another approach would be to use the animals themselves as background points (Corcoran & Hedrick,

347   2019).

5. Conclusions

349   Technological development is driving price reductions and capability expansion in thermal and high-

350   speed cameras, along with supporting equipment such as UAVs. However, the software required to

351   make full use of these capabilities for research in fields as diverse as biomechanics, animal behavior,

352   ecology, and population monitoring remains the province of specialized workflows in individual lab

353   groups. ThuTracker provides an integrated, graphical, and user-friendly package to fill these needs, thus

354   expanding the number of researchers able to make effective use of these emerging technologies.

Acknowledgements

355

356   We thank Bethany Straw from the National Renewable Energy Laboratory for help with deploying

357   thermal cameras. Iwona Kuczynska and Shelly Colatskie provided videos of gray bats exiting caves.

358   William Valentine assisted with code development. Kacie Quigley, Madison Simmons and Jonas

359   Håkansson conducted manual counts of bat exits from bridge and cave videos and Jonas Håkansson

360   provided useful feedback on an earlier version of this manuscript.

Funding

361

Authors' Contributions

364

365   A.C. and T.H conceived of and developed the software. M.S. provided funding and guided software

366   development. E.B. collected data used for testing and aided with data analysis. A.C. drafted the

367   manuscript and all authors edited the manuscript and gave final approval for the publication.

Data Availability Statement

368

369   ThruTracker installation files, a user manual and software tutorials are available at

370   www.sonarjamming.com/thruTracker. Source code is available as a GitHub repository

371   (https://github.com/AaronJCorcoran/ThruTracker).

372   References

373   Abdel-Aziz, Y. I., & Karara, H. M. (1971). Direct linear transformation from comparator coordinates into

374   object space coordinates in close-range photogrammetry. In *Proceedings of the Symposium on*

375   *Close Range Photogrammetry* (pp. 1–18). American Society for Photogrammetry and Remote

376   Sensing. doi:10.14358/PERS.81.2.103

377   Arnett, E. B., & Baerwald, E. F. (2013). Impacts of Wind Energy Development on Bats: Implications for

378   Conservation. In R. Adams & S. Pederson (Eds.), *Bat Evolution, Ecology, and Conservation* (pp. 435–

379   456). New York: Springer. doi:10.1007/978-1-4614-7397-8

380   Ballerini, M., Cabibbo, N., Candelier, R., Cavagna, A., Cisbani, E., Giardina, I., … Zdravkovic, V. (2008).

381   Interaction ruling animal collective behavior depends on topological rather than metric distance:

382   Evidence from a field study. *Proceedings of the National Academy of Sciences of the United States*

383   *of America*, *105*(4), 1232–1237. doi:10.1073/pnas.0711437105

384   Betke, M., Hirsh, D. E., Makris, N. C., McCracken, G. F., Procopio, M., Hristov, N. I., … Others. (2008).

385   Thermal imaging reveals significantly smaller Brazilian free-tailed bat colonies than previously

386   estimated. *Journal of Mammalogy*, *89*(1), 18–24.

387   Bouguet, J.-Y. (1999). *Visual methods for three-dimensional modeling*. Cal Tech. *PhD Dissertation*

388   https://resolver.caltech.edu/CaltechETD:etd-02072008-115723

389   Christiansen, P., Steen, K., Jørgensen, R., & Karstoft, H. (2014). Automated Detection and Recognition of

390   Wildlife Using Thermal Cameras. *Sensors*, *14*(8), 13778–13793. doi:10.3390/s140813778

391   Cilulko, J., Janiszewski, P., Bogdaszewski, M., & Szczygielska, E. (2013, February). Infrared thermal

392   imaging in studies of wild animals. *European Journal of Wildlife Research*. Springer Verlag.

393   doi:10.1007/s10344-012-0688-1

394   Corcoran, A. J., & Hedrick, T. L. (2019). Compound-v formations in shorebird flocks. *ELife*, *8*.

395   doi:10.7554/eLife.45071

396   Cryan, P. M., Gorresen, P. M., Hein, C. D., Schirmacher, M. R., Diehl, R. H., Huso, M. M., … Dalton, D. C.

397   (2014). Behavior of bats at wind turbines. *Proceedings of the National Academy of Sciences of the*

398   *United States of America*, *111*(42), 15126–31. doi:10.1073/pnas.1406672111

399   Cullinan, V. I., Matzner, S., & Duberstein, C. A. (2015). Classification of birds and bats using flight tracks.

400   *Ecological Informatics*, *27*, 55–63. doi:10.1016/j.ecoinf.2015.03.004

401   Dell, A. I., Bender, J. A., Branson, K., Couzin, I. D., de Polavieja, G. G., Noldus, L. P. J. J., … Brose, U. (2014,

402   July). Automated image-based tracking and its application in ecology. *Trends in Ecology and*

403   *Evolution*. Elsevier Ltd. doi:10.1016/j.tree.2014.05.004

404   Evangelista, D. J., Ray, D. D., Raja, S. K., & Hedrick, T. L. (2017). Three-dimensional trajectories and

405   network analyses of group behaviour within chimney swift flocks during approaches to the roost.

406   *Proceedings of the Royal Society B. Biological Sciences*, *284*(1849), 20162602.

407   doi:10.1098/rspb.2016.2602

408   Gauthreaux, S. A., & Livingston, J. W. (2006). Monitoring bird migration with a fixed-beam radar and a

409   thermal-imaging camera. *Journal of Field Ornithology*, *77*(3), 319–328. doi:10.1111/j.1557-

410   9263.2006.00060.x

411   Gonzalez, L., Montes, G., Puig, E., Johnson, S., Mengersen, K., & Gaston, K. (2016). Unmanned aerial

412   vehicles (UAVs) and artificial intelligence revolutionizing wildlife monitoring and conservation.

413   *Sensors*, *16*(1), 97. doi:10.3390/s16010097

414   Hartley, R., & Zisserman, A. (2004). *Multiple View Geometry in Computer Vision*. Cambridge University

415   Press. doi:10.1017/cbo9780511811685

416   Hedrick, T. L. (2008). Software techniques for two- and three-dimensional kinematic measurements of

417   biological and biomimetic systems. *Bioinspiration and Biomimetics*, *3*(3), 6. doi:10.1088/1748-

418   3182/3/3/034001

419   Horn, J. W., Arnett, E. B., & Kunz, T. H. (2008). Behavioral Responses of Bats to Operating Wind Turbines.

420   *Journal of Wildlife Management*, *72*(1), 123–132. doi:10.2193/2006-465

421   Horton, K. G., Shriver, W. G., & Buler, J. J. (2015). A comparison of traffic estimates of nocturnal flying

422   animals using radar, thermal imaging, and acoustic recording. *Ecological Applications*, *25*(2), 390–

423   401. doi:10.1890/14-0279.1.sm

424   Jackson, B. E., Evangelista, D. J., Ray, D. D., & Hedrick, T. L. (2016). 3-D for the people: Multi-camera

425   motion capture in the field with consumer-grade cameras and open source software. *Biology*

426   *Open*, *5*(9), 1334–1342. doi:10.1242/bio.018713

427   Jolles, J. W., Boogert, N. J., Sridhar, V. H., Couzin, I. D., & Manica, A. (2017). Consistent individual

428   differences drive collective behavior and group functioning of schooling fish. *Current Biology*,

429   *27*(18), 2862-2868.e7. doi:10.1016/j.cub.2017.08.004

430   Kinzie, K., Hale, A., Bennett, V., Romano, B., Skalski, J., Coppinger, K., & Miller, M. F. (2018). Ultrasonic

431   Bat Deterrent Technology. Technical Report DE-EE007035 doi:/10.2172/1484770

432   Knorlein, B. J., Baier, D. B., Gatesy, S. M., Laurence-Chasen, J. D., & Brainerd, E. L. (2016). Validation of

433   XMALab software for marker-based XROMM. *Journal of Experimental Biology*, *219*(23), 3701–3711.

434   doi:10.1242/jeb.145383

435   Kuhn, H. W. (1955). The Hungarian method for the assignment problem. *Naval Research Logistics*

436   *Quarterly*, *2*(1–2), 83–97. doi:10.1002/nav.3800020109

437   Kunz, T. H., Betke, M., Hristov, N. I., & Vonhof, M. J. (2009). Methods for assessing colony size, and

438   relative abundance of bats. In T. H. Kunz & S. Parsons (Eds.), *Ecological and Behavioural Methods*

439   *for the Study of Bats* (pp. 133–157). Baltimore, MD: Johns Hopkins University Press.

440   Lourakis, M. I. A., & Argyros, A. A. (2009). SBA: A software package for generic sparse bundle

441   adjustment. *ACM Transactions on Mathematical Software*, *36*(1), 1–30.

442   doi:10.1145/1486525.1486527

443   Mathis, A., Mamidanna, P., Cury, K. M., Abe, T., Murthy, V. N., Mathis, M. W., & Bethge, M. (2018).

444   DeepLabCut: markerless pose estimation of user-defined body parts with deep learning. *Nature*

445   *Neuroscience*, *21*(9), 1281–1289. doi:10.1038/s41593-018-0209-y

446   Matzner, S., Cullinan, V. I., & Duberstein, C. A. (2015). Two-dimensional thermal video analysis of

447   offshore bird and bat flight. *Ecological Informatics*, *30*, 20–28. doi:10.1016/J.ECOINF.2015.09.001

448   Matzner, S., Warfel, T., & Hull, R. (2020). ThermalTracker-3-D: A thermal stereo vision system for

449   quantifying bird and bat activity at offshore wind energy sites. *Ecological Informatics*, *57*, 101069.

450   doi:10.1016/J.ECOINF.2020.101069

451   Narendra, A., & Ramirez-Esquivel, F. (2017). Subtle changes in the landmark panorama disrupt visual

452   navigation in a nocturnal bull ant. *Philosophical Transactions of the Royal Society B: Biological*

453   *Sciences*, *372*(1717). doi:10.1098/rstb.2016.0068

454   Nath, T., Mathis, A., Chen, A. C., Patel, A., Bethge, M., & Mathis, M. W. (2019). Using DeepLabCut for 3-D

455   markerless pose estimation across species and behaviors. *Nature Protocols*, *14*(7), 2152–2176.

456   doi:10.1038/s41596-019-0176-0

457   Noldus, L. P. J. J., Spink, A. J., & Tegelenbosch, R. A. J. (2001). EthoVision: A versatile video tracking

458   system for automation of behavioral experiments. *Behavior Research Methods, Instruments, and*

459   *Computers*, *33*(3), 398–414. doi:10.3758/BF03195394

460   Pereira, T. D., Aldarondo, D. E., Willmore, L., Kislin, M., Wang, S. S. H., Murthy, M., & Shaevitz, J. W.

461   (2019). Fast animal pose estimation using deep neural networks. *Nature Methods*, *16*(1), 117–125.

462   doi:10.1038/s41592-018-0234-5

463   Pérez-Escudero, A., Vicente-Page, J., Hinz, R. C., Arganda, S., & De Polavieja, G. G. (2014). IdTracker:

464   Tracking individuals in a group by automatic identification of unmarked animals. *Nature Methods*,

465   *11*(7), 743–748. doi:10.1038/nmeth.2994

466   Rodriguez, A., Zhang, H., Klaminder, J., Brodin, T., Andersson, P. L., & Andersson, M. (2018). *ToxTrac* : A

467   fast and robust software for tracking organisms. *Methods in Ecology and Evolution*, *9*(3), 460–464.

468   doi:10.1111/2041-210X.12874

469   Ronconi, R. A., Allard, K. A., & Taylor, P. D. (2015, January 1). Bird interactions with offshore oil and gas

470   platforms: Review of impacts and monitoring techniques. *Journal of Environmental Management*.

471   Academic Press. doi:10.1016/j.jenvman.2014.07.031

472   Schirmacher, M. (2020). Evaluating the effectiveness of an ultrasonic acoustic deterrent in reducing bat

473   fatalities at wind energy facilities.Technical Report DOE-BCI-0007036

474   Schönberger, J. L., & Frahm, J.-M. (2016). Structure-from-Motion Revisited. In *Proceedings of the IEEE*

475   *Conference on Computer Vision and Pattern Recognition (CVPR)* (pp. 4104–4113).

476   Seymour, A. C., Dale, J., Hammill, M., Halpin, P. N., & Johnston, D. W. (2017). Automated detection and

477   enumeration of marine wildlife using unmanned aircraft systems (UAS) and thermal imagery.

478   *Scientific Reports*, *7*(1), 1–10. doi:10.1038/srep45127

479   Shelton, R. M., Jackson, B. E., & Hedrick, T. L. (2014). The mechanics and behavior of cliff swallows

480   during tandem flights. *Journal of Experimental Biology*, *217*(15).

481   Sholtis, K. M., Shelton, R. M., & Hedrick, T. L. (2015). Field Flight Dynamics of hummingbirds during

482   territory encroachment and defense. *PLOS ONE*, *10*(6), e0125659.

483   doi:10.1371/journal.pone.0125659

484   Sridhar, V. H., Roche, D. G., & Gingins, S. (2019). Tracktor: Image-based automated tracking of animal

485   movement and behaviour. *Methods in Ecology and Evolution*, *10*(6), 815–820. doi:10.1111/2041-

486   210X.13166

487   Theriault, D. H., Fuller, N. W., Jackson, B. E., Bluhm, E., Evangelista, D., Wu, Z., … Hedrick, T. L. (2014). A

488   protocol and calibration method for accurate multi-camera field videography. *Journal of*

489   *Experimental Biology*, *217*(11).

490   Yahyanejad, S., Misiorny, J., & Rinner, B. (2011). Lens distortion correction for thermal cameras to

491   improve aerial imaging with small-scale UAVs. In *ROSE 2011 - IEEE International Symposium on*

492   *Robotic and Sensors Environments, Proceedings* (pp. 231–236). doi:10.1109/ROSE.2011.6058528

493   Zhang, Z. (2000). A flexible new technique for camera calibration. *IEEE Transactions on Pattern Analysis*

494   *and Machine Intelligence*, *22*(11), 1330–1334. doi:10.1109/34.888718

495   Zivkovic, Z. (2004). Improved adaptive Gaussian mixture model for background subtraction. In

496   *Proceedings - International Conference on Pattern Recognition* (Vol. 2, pp. 28–31). Institute of

497   Electrical and Electronics Engineers Inc. doi:10.1109/icpr.2004.1333992

498   Zivkovic, Z., & Van Der Heijden, F. (2006). Efficient adaptive density estimation per image pixel for the

499   task of background subtraction. *Pattern Recognition Letters*, *27*(7), 773–780.

500   doi:10.1016/j.patrec.2005.11.005

501